A bacterial thioester domain functions as a pH-responsive covalent adhesion module

Yuki Tokunaga[1], Ryo Matsunaga[1,2*], Hiroko Kozuka-Hata[3], Masaaki Oyama[3], Kouhei Tsumoto[1,2,3*]

[1]Department of Bioengineering, School of Engineering, The University of Tokyo, 7-3-1 Hongo, Bunkyo-ku, Tokyo, 113-8656, Japan

[2]Department of Chemistry and Biotechnology, School of Engineering, The University of Tokyo, 7-3-1 Hongo, Bunkyo-ku, Tokyo, 113-8656, Japan

[3]The Institute of Medical Science, The University of Tokyo, 4-6-1 Shirokanedai, Minato-ku, Tokyo, 108-8639, Japan

*Correspondence: *ryo-matsunaga@g.ecc.u-tokyo.ac.jp* and *tsumoto@bioeng.t.u-tokyo.ac.jp*

Abstract

Thioester domains (TEDs) represent a family of bacterial adhesin domains that mediate covalent anchoring to target ligands via an intramolecular thioester bond. Although the broad distribution of TEDs among Gram-positive bacteria suggests a critical functional role, the biological significance of this covalent mechanism remains unclear. In this study, we demonstrated that TED-mediated covalent anchoring is reversible and that its equilibrium is regulated by pH. Specifically, SfbI-TED from Group A *Streptococcus* binds tightly to fibrinogen at physiological pH, whereas mild acidification to pH 6.0 induces rapid dissociation of the complex. Thermodynamic analyses revealed that this pH-responsiveness arises from the intrinsic properties of the thioester bond within the TED. Similar pH-dependent behavior was observed in phylogenetically distinct TEDs, suggesting that pH-responsive adhesion is a conserved feature of the TED family across Gram-positive bacteria.

Throughout the progression of infection, pathogenic bacteria encounter dynamic changes in the host environment to which they deploy distinct strategies depending on the stage of infection. Among the environmental factors that influence bacterial physiology, pH is a critical determinant of virulence. For instance, Group A *Streptococcus* (GAS) encounters heterogeneous pH microenvironments, typically ranging from mildly acidic (~pH 5.8) to near-neutral (pH 7.4), across various infection phases, such as initial pharyngeal attachment, biofilm formation, and invasion of deeper tissues[1–3]. To adapt to these pH variations, GAS utilizes several pH-responsive regulators (*e.g.*, CovR/S[4,5], CiaH/CiaR[6], and RopB[7]) to modulate the expression of virulence factors, including adhesins, capsules, streptokinases, and various toxins[3,7,8]. Although such gene-regulatory circuits have been the primary focus of research on bacterial pH responses[7,9], it is equally crucial to elucidate how the function of expressed proteins is modulated by environmental pH. In particular, pH-dependent functional modulation of host-interacting surface proteins, such as adhesins, has been characterized in only a limited number of systems and remains poorly understood[10–14].

In this study, we investigated the pH-responsiveness of the thioester domain (TED), a family of adhesin domains prevalent among Gram-positive bacteria across the phyla *Firmicutes* and *Actinobacteria*[15,16]. First reported in 2010[17], the TED has a unique ability to spontaneously form an intramolecular thioester bond between the conserved cysteine and glutamine side chains[15,17]. Given that a C426A mutation in Cpa-TED–which prevents thioester formation–results in a ~75% reduction in adhesion to keratinocytes[17], it was postulated that TEDs covalently anchor bacteria to host cells by reacting their internal thioester with a nucleophile on the host surface[15,17]. Drawing on an analogy to the mammalian complement proteins C3 and C4, which utilize similar Cys–Gln thioesters to form covalent linkages with their targets, investigators initially presumed TED-mediated binding to be irreversible[15].

Walden *et al.* subsequently identified a TED within the fibronectin-binding protein SfbI[15], a GAS adhesin causing cell adhesion and invasion. Using mass spectrometry, they demonstrated that the SfbI-TED and its

target, fibrinogen, form a complex that is cross-linked via an intermolecular isopeptide bond. This crosslinking results from an acyl-transfer reaction, driven by the nucleophilic attack of an amine group from fibrinogen on the TED thioester. They termed this mechanism a "chemical harpoon" and proposed that it facilitates irreversible bacterial attachment to the host. Notably, unlike complement proteins C3 and C4, which utilize thioester-mediated crosslinking to react with a broad range of nucleophiles, TEDs exhibit remarkable target specificity. Walden *et al.* examined the binding of fibrinogen to ten distinct TEDs and found that only SfbI- and FbaB-TED, both encoded within the FCT region of the GAS genome[18], were capable of binding fibrinogen. Moreover, mass spectrometry revealed that SfbI-TED specifically reacts with Lys100 on the fibrinogen Aα chain, differentiating it from the other available lysine residues. This finding indicates that the "chemical harpoon" mechanism involves a targeted recognition mechanism rather than a random nucleophilic attack on a reactive thioester[15].

Recently, Echelman and Alonso-Caballero challenged the current view that TED-mediated chemistry is irreversible[19,20]. Using single-molecule force spectroscopy, they demonstrated that the Cpa thioester can be cleaved by a small-molecule nucleophile (methylamine) and reforms upon removal of the nucleophile, provided that the mechanical load is sufficiently low to permit TED refolding. These findings suggest that thioester reactivity is gated by the structural integrity of the TED fold, leading to the proposal of a "smart covalent bond" model in which the lifetime of the covalent linkage is modulated by mechanical force. However, these experiments relied on small-molecule amines rather than on physiological protein targets. Consequently, it remains to be elucidated whether intermolecular crosslinking between TEDs and their native ligands is similarly reversible[19,20].

Using SfbI-TED as a model system, we analyzed the kinetic and thermodynamic mechanisms underlying target recognition and crosslinking. Biolayer interferometry revealed a multistep binding process: initial non-covalent recognition, followed by thioester-mediated formation of an intermolecular crosslink, which is in

dynamic equilibrium with the reverse reaction. Furthermore, we discovered that SfbI-TED displayed pronounced pH-responsive behavior; specifically, the SfbI-TED/fibrinogen complex dissociated rapidly under mildly acidic conditions (~pH 6.0). Similar pH-dependent properties were observed in other TED homologues, suggesting that pH responsiveness is a conserved feature of the TED family rather than a unique attribute of SfbI. These observations suggest that the ability to function as a pH-responsive adhesin module may have contributed to the widespread dissemination and evolutionary success of TEDs in Gram-positive bacteria.

Results

pH-dependent changes in thermal stability

To characterize SfbI-TED, we first examined the pH dependence of its thermal stability. Previous work on Cpa indicated that the intramolecular thioester bond contributes to adhesion, but not to thermal stability; the melting temperature (T_m) did not change in a thioester-deficient mutant[21]. Therefore, we compared wild-type SfbI-TED with thioester-deficient mutants (Q261A, C109S, and C109A). Differential scanning calorimetry (DSC) revealed a marked pH dependence exclusively for the wild type (Fig. 1a,b). At pH 7.3, the T_m of the wild type (52.10 °C) was comparable to that of the Q261A mutant (53.44 °C), which lacks the thioester bond, consistent with the previous report. However, as the pH decreased, an additional denaturation peak appeared around 65 °C specifically in the wild type; this higher-temperature peak became dominant as the pH declined. We attribute this behavior to the coexistence of molecules with an intact and cleaved thioester bond within the wild-type sample; the former gives rise to a higher-temperature peak and the latter to a lower-temperature peak. This interpretation is reinforced by the observation that the T_m values of all thioester-deficient mutants correspond to the lower-temperature peak of the wild-type at each pH.

In all samples, including the mutants, thermograms shifted by about 2–5 °C between pH 6.0 and 7.3, indicating a small pH-dependent fluctuation even in the absence of the thioester bond (Extended Data Table. 1). To investigate whether pH affects structural conformation or packing, we measured the circular dichroism (CD) spectra at pH 6.0 and 7.4 (Fig. 1c). The spectra varied between pH conditions, primarily in the magnitude of the minimum at 208 nm. However, no clear change was observed in the ellipticity at 222 nm (reflecting α-helical content), or at 217 nm (reflecting β-sheet content)[22]. The ellipticity at 208 nm is highly sensitive to the relative orientation of the helices[23,24], suggesting that SfbI-TED undergoes minor pH-dependent changes in the packing of its helical subdomain. This observation is consistent with the small (2–5 °C) shift in the DSC thermograms seen for all mutants, independent of the thioester bond (Fig. 1a,b).

1

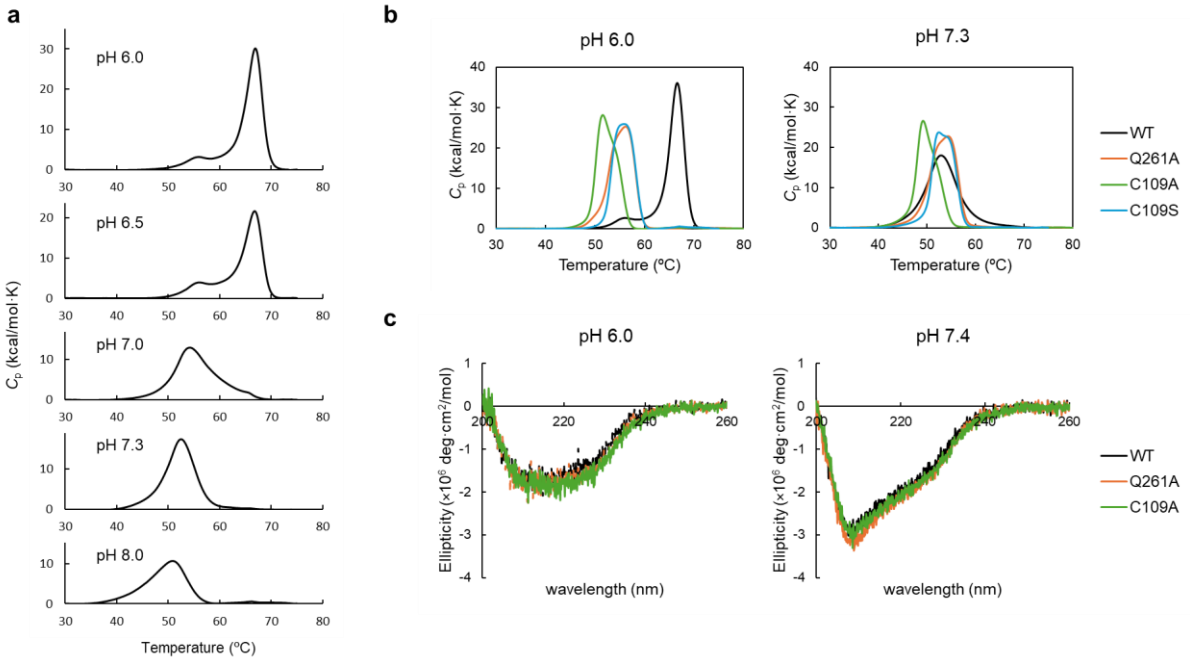

2

Fig. 1 | pH-dependent structural properties of SfbI-TED.
a, Thermal stability of SfbI-TED analyzed by DSC. The thermograms show the molar heat capacity (C_p) as a function of temperature across a pH range of 6.0–8.0. **b,** Comparison of DSC profiles between wild-type SfbI-TED and thioester-deficient mutants (C109A, C109S, and Q261A) at pH 6.0 and 7.4. **c**, Far-UV CD spectra of SfbI-TED at pH 6.0 and 7.4.

3

4

pH-dependent cleavage and reformation of the thioester bond

To determine whether molecules with cleaved and intact thioester bonds coexist and whether their ratio changes with pH, we quantified free thiols using 4,4'-dithiodipyridine (4-PDS). This reagent reacts specifically with thiols to release 4-thiopyridone (4-TP; ε_{324} = 21,400 M^{-1} cm^{-1})[25] (Fig. 2a). Although the reaction between low-molecular-weight thiols and 4-PDS is typically rapid, we observed it to be extremely slow with folded SfbI-TED (Extended Data Fig. 1), suggesting that steric hindrance restricts the accessibility of 4-PDS. Consequently, we performed the reaction under denaturing conditions (Fig. 2b). We mixed SfbI-TED and sufficient 4-PDS at room temperature and rapidly heated to denature the TED fold. After rapid cooling and removal of aggregates, the absorbance at 324 nm (A_{324}) was measured. Given that the side chain of C109 is the sole thiol in SfbI-TED, all thiols quantified in this assay were attributed to thioester bond cleavage. Normalized A_{324} (%) was calculated by dividing the observed A_{324} by the value expected for complete thioester-bond cleavage in the protein.

Given that the thioester bond is generally stable under acidic and neutral conditions (with a hydrolysis half-life of ~20,000 h at pH 7.0[26]), the observed A_{324} values are most consistent with the thioester bond being pre-cleaved within the folded state.

As expected, the Q261A mutant, which lacks a thioester bond, showed nearly 100% normalized A_{324} at both pH 6.0 and 7.3. In contrast, the wild type exhibited marked pH dependence, with normalized A_{324} values being $6.5 \pm 1.1\%$ (mean $\pm$ s.d., $n = 3$) at pH 6.0 and $51.5 \pm 8.8\%$ at pH 7.3 (Fig. 2c,d). Importantly, this pH dependence persisted even after repeated dialysis between pH 6.0 and 7.3 (Extended Data Fig. 2), demonstrating a reversible equilibrium between the cleaved and intact states of the intramolecular thioester bond.

The finding that thioester bond cleavage is promoted at higher pH is consistent with the DSC results. The

apparent discrepancy between the ~50% cleavage at pH 7.3 observed in the thiol assay and the single lower-temperature DSC peak at pH 7.3 can be reconciled by the difference in heating rates; the thiol assay employs a rapid ramp (210 °C /min), whereas DSC uses a slow ramp (1 °C /min). In the 50–60 °C range, molecules with intact thioester bonds remained folded, whereas those with cleaved thioester bonds rapidly unfolded (Fig. 1a) and were therefore removed from the equilibrium between cleavage and reformation. Consequently, slower heating in the DSC allowed more extensive thioester bond cleavage to occur during the transition. The broader width of the lower-temperature DSC peak relative to the higher-temperature peak was also consistent with a Poisson-like process in which thioester bond cleavage is the rate-limiting event for unfolding.

In our experimental system, low-molecular-weight amines were absent, making hydrolysis a plausible mechanism for thioester cleavage. Indeed, mass spectrometry detected a peptide containing a Q261E conversion, which is indicative of thioester bond hydrolysis (Extended Data Fig. 3). Although only a single peptide containing Q261E was detected in our experiment, its strong negative charge (four acidic and one basic residue) likely reduced the ionization efficiency in the nano LC-MS/MS measurements. Collectively, these results support the occurrence of hydrolytic thioester bond cleavage.

The hypothesis that histidine protonation drives pH-dependent behavior was tested using the H93A mutant, in which the sole histidine in SfbI-TED is substituted with alanine. Thiol quantification showed a pH dependence similar to that of the wildtype (Fig. 2d), indicating that H93 protonation was not involved.

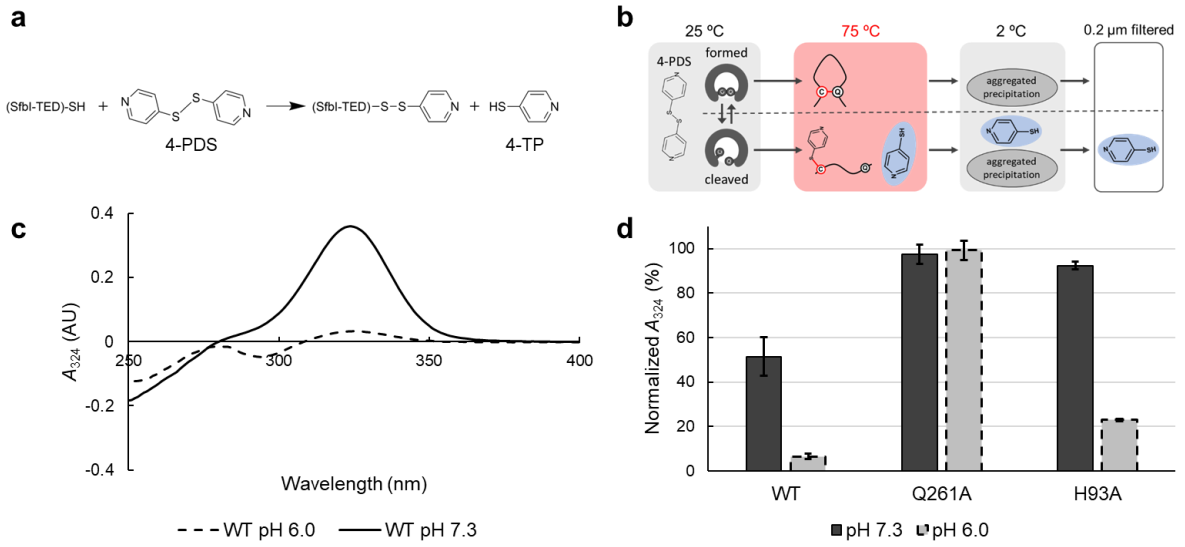

Fig. 2 | Quantification of intramolecular thioester bond cleavage.
a, Reaction scheme of thiol quantification using 4-PDS. 4-PDS reacts specifically with free thiols to release 4-TP, which absorbs light at 324 nm. **b,** Schematic of the denaturation-based thiol quantification assay. SfbI-TED was incubated with 4-PDS, heat-denatured to expose an internal thiol from a cleaved thioester, and rapidly cooled. Aggregates were removed by filtration prior to absorbance measurement. **c,** Absorbance spectra of the reaction mixtures at pH 6.0 and 7.3 under denaturing conditions. **d,** pH-dependent cleavage of the thioester bond. Normalized A_{324} represents the fraction of molecules with a cleaved thioester bond relative to the theoretical maximum (calculated for 30 µM SfbI-TED). Data are presented as mean ± s.d. (n=3).

Model of SfbI-TED binding to fibrinogen

Using mass spectrometry, Walden et al. demonstrated that SfbI-TED binds specifically to Lys100 on the fibrinogen Aα chain[15]. Given that the reaction between a thioester bond and a lysine side-chain amine is, in principle, a generic nucleophilic acyl transfer, such specificity must stem from an additional mechanism: a protein–protein interaction that recognizes the local environment of Lys100. To account for this, we hypothesized a two-step reaction model wherein the surface residues of SfbI-TED first recognize the local environment of Lys100 on fibrinogen through non-covalent interactions, followed by thioester-mediated crosslinking:

$$\text{SfbI-TED} + \text{Fg} \underset{k_{\text{off}}}{\overset{k_{\text{on}}}{\rightleftharpoons}} \text{Complex}_{\text{non-covalent}} \xrightarrow{k_{\text{c}}} \text{Complex}_{\text{covalent}}$$

To validate this model, we measured the interaction between fibrinogen and SfbI-TED using bio-layer interferometry (BLI). SfbI-TED was immobilized on the biosensor, which was subsequently immersed in fibrinogen solutions to monitor binding. The C109A mutant showed no detectable binding, whereas the Q261A mutant exhibited distinct interaction with fibrinogen (Extended Data Fig. 4). This interaction demonstrates that SfbI-TED retains the capacity for non-covalent recognition of fibrinogen even in the absence of an intact thioester bond, validating that the model comprises at least two steps for the overall adhesion process.

Therefore, in this reaction model, the BLI response comprises contributions from both non-covalent and covalent species. To distinguish between these components, we applied a strong wash (pH 2.0) after the dissociation step. Under this condition, the response of the Q261A mutant, which is unable to form an intermolecular crosslink, was completely abolished, whereas the signal for the wildtype remained largely unchanged (Fig. 3a). These results indicate that the residual response after the pH 2.0 wash is attributable to the covalent crosslinked complex. When the pH 2.0 wash was applied immediately post-association, the response persisted (Extended Data Fig. 5). This confirms that a covalent linkage is formed upon association; the decrease in the response observed in the dissociation phase implies that the covalent crosslink is

reversibly cleaved. This finding supports the reversible crosslinking hypothesis proposed by Echelman *et al.*[19,20], showing that it also applies to interactions with a physiological target. Based on these findings, we reformulated the following binding model:

$$\text{SfbI-TED} + \text{Fg} \underset{k_{\text{off}}}{\overset{k_{\text{on}}}{\rightleftharpoons}} \text{Complex}_{\text{non-covalent}} \underset{k_{\text{c,rev}}}{\overset{k_{\text{c}}}{\rightleftharpoons}} \text{Complex}_{\text{covalent}}$$

The dissociation of this covalent complex is likely driven by the reversal of the crosslinking reaction; the intermolecular isopeptide bond undergoes nucleophilic attack by the cysteine side chain of TED, resulting in bond cleavage and reformation of the intramolecular thioester bond within TED (Fig. 3c). Echelman *et al.* demonstrated that the thioester bond of Cpa-TED loses its reactivity toward methylamine when TED is unfolded under mechanical force[19,20]. These findings indicate that both the acyl transfer reaction and its reversal (Fig. 3c) are catalyzed by structural features intrinsic to the TED fold.

Dissociation of the crosslinked complex at mildly acidic pH

Based on our finding that the intramolecular thioester bond of SfbI-TED undergoes pH-dependent cleavage, we examined whether its interaction with fibrinogen was pH-dependent. Following the association step at pH 7.3, the sensor was transferred into dissociation buffers with varying pH values (Fig. 3a,b). The Q261A mutant, which cannot form an intermolecular crosslink, showed no dependence on pH during dissociation, whereas the wild-type complex dissociated faster at lower pH. These results indicate that non-covalent interactions are insensitive to pH, whereas the equilibrium governing the formation and cleavage of the intermolecular crosslink is strongly influenced by pH. Furthermore, the observation that SfbI-TED, following the dissociation of fibrinogen at pH 6.0, could repeatedly form a covalently crosslinked complex upon rebinding to fibrinogen (Extended Data Fig. 5) is consistent with our reaction model, wherein cleavage of the intermolecular crosslink is coupled with reformation of the intramolecular thioester bond (Fig. 3c).

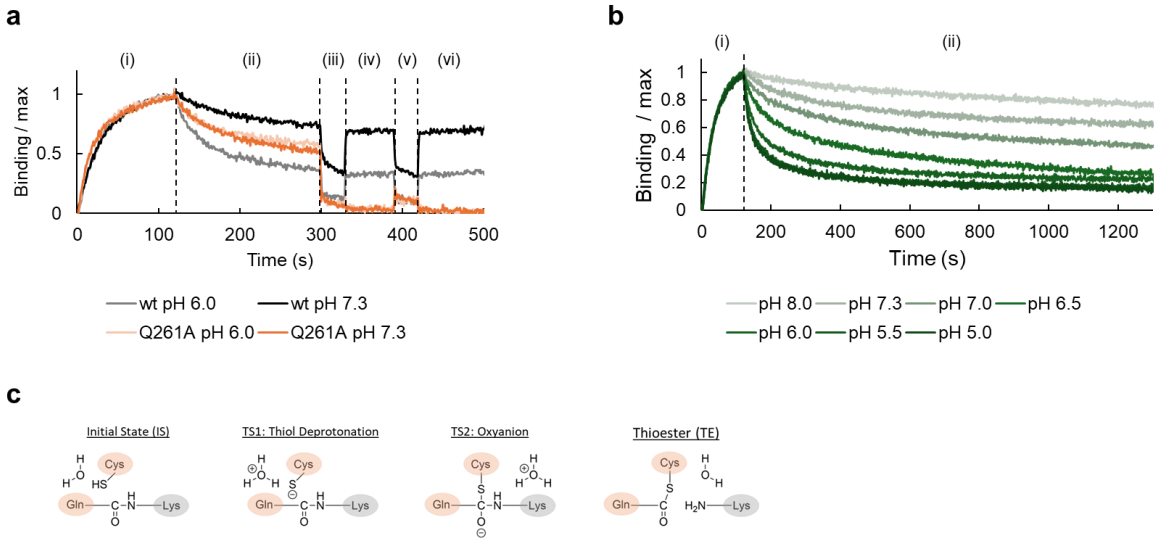

Fig. 3 | Kinetic mechanism of pH-dependent covalent binding.
a, Validation of covalent crosslinking by BLI. The sensorgrams display the sequential kinetic steps consisting of (i) association with fibrinogen in pH 7.3, (ii) dissociation in either pH 7.3 or pH 6.0, (iii)(v) strong wash in pH 2.0, and (iv)(vi) neutralization in pH 7.3. The vertical axis represents the response normalized to the maximum value in the association step. **b**, pH-dependent dissociation profiles. The sensorgrams display the kinetic response consisting of (i) an association phase with fibrinogen at pH 7.3, followed by (ii) a dissociation phase triggered by transferring the sensors into running buffers ranging from pH 5.0 to 8.0. **c**, Schematic of the proposed cleavage reaction of the intermolecular isopeptide bond formed between SfbI-TED (orange) and fibrinogen (gray).

Identification of SfbI-TED residues involved in target recognition

Previous mass-spectrometric analysis established that SfbI-TED forms an intermolecular crosslink with Lys100 on the fibrinogen Aα chain[15]. To gain structural insight into the binding pose, we predicted the complex structure using AlphaFold 3, incorporating the coiled-coil region of fibrinogen encompassing Lys100[27]. Across 500 structures generated from 100 random seeds, the interface predicted Template Modeling (ipTM) scores were generally low (Fig. S1); however, 260 models placed SfbI-TED in close vicinity to Lys100. In these 260 models, the average distance between the carbonyl carbon atom of the TED thioester and the nitrogen atom of the Lys100 side-chain amine was 3.4 Å, with minimum distance of 2.3 Å (the model exhibiting the closest proximity between the reactive groups is shown in Fig. 4a).

In the generated structures, the three loops of SfbI-TED formed a binding interface with fibrinogen. To experimentally validate their contribution, we performed a high-throughput single-mutant analysis using the FASTIA method[28]. We targeted the 37 residues located on these loops. For the construct design, A90 was mutated to Trp, and owing to the failure to express D83A, the D83N mutant was substituted. Each mutant was immobilized on a BLI sensor and sequentially exposed to fibrinogen at 25, 100, 400, and 1600 nM (pH 7.3). The resulting sensorgrams were globally fitted to the two-step model to obtain kinetic parameters ($k_{\mathrm{on}}, k_{\mathrm{off}}, k_{\mathrm{c}}, k_{\mathrm{c,rev}}$) (Fig. S2,S3). Notably, the H93A mutant did not bind. Although the H93F mutant was constructed subsequently, it failed to bind in a similar manner.

From the kinetic parameters obtained by fitting, the reaction free energies (ΔG) for each step of the binding model were calculated (Fig. 4b), and the change in the free energy of the non-covalent interaction ($\Delta\Delta G_{\mathrm{non\text{-}covalent}}$) was mapped onto the surface of SfbI-TED (Fig. 4c). Red residues corresponded to mutations that decrease the affinity, indicating a strong contribution of native side chains to target recognition. Only four residues showed a reduction in affinity corresponding to a $\Delta\Delta G_{\mathrm{non\text{-}covalent}}$ of more than 1 kcal/mol, and complete loss of binding was observed exclusively for the H93A/F mutations (Fig. S2). Thus, non-covalent

target recognition by SfbI-TED was primarily mediated by the hotspot residue H93 ($\Delta\Delta G_{\text{non-covalent}} > 2\ \text{kcal/mol}$)[29], together with auxiliary interactions contributed by L112, Y115, and R118, which cluster around H93. In contrast, loop 3 was not involved in fibrinogen binding. Loops 1 and 2 flank the intramolecular thioester bond and their dominant contribution to fibrinogen recognition is consistent with the structural arrangement of the domain.

A notable intrinsic property of TED is the positive correlation between the free energies of the two-step reactions, with a Pearson correlation coefficient of 0.67 (Fig. 4b; see Methods and Fig. S4 and S5 for the assessment). This result suggests that stabilization of the covalent complex necessitates the formation of a sufficiently stable non-covalent complex. This phenomenon is consistent with previous studies showing that TEDs can spontaneously reform their intramolecular thioester bonds, facilitating disengagement from unproductive reactions with small amines that are abundant *in vivo*[19,20,30].

During the course of our single-mutant analysis, we identified two mutants, F116Y and L112T, which bound more strongly than the wild type (Fig. 4d). Both mutants markedly stabilized the covalent complex, with L112T exhibiting almost irreversible binding. Although these mutations also slowed dissociation at pH 6.0, they retained the characteristic pH dependence observed in the wild type, wherein dissociation was accelerated under acidic conditions.

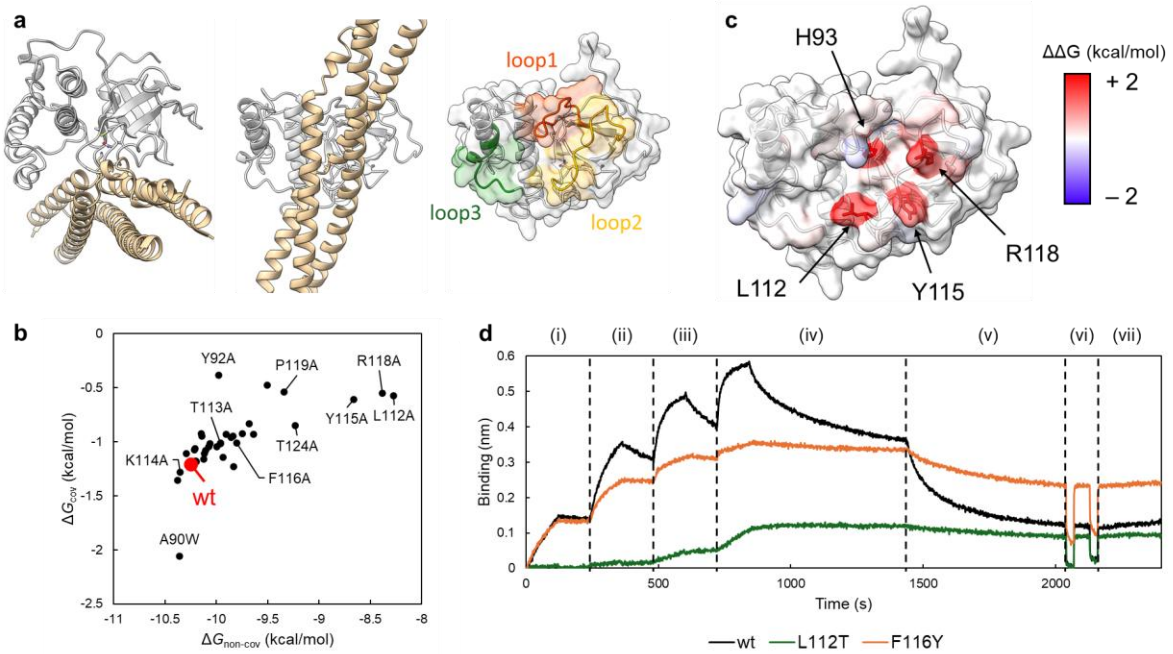

Fig. 4 | Residue-level contributions to SfbI-TED target recognition.
a, Structural model of the SfbI-TED–fibrinogen complex predicted by AlphaFold 3. SfbI-TED and fibrinogen are colored white and ochre, respectively. The side chains of C109 and Q261, which form the thioester bond, and the target lysine (K100) on fibrinogen are shown as sticks. The right panel highlights loop 1–3 at the putative binding interface, which were subjected to single-mutant analysis. **b,** Correlation between the free energies of non-covalent association ($\Delta G_{\text{non-cov}}$) and covalent crosslinking (ΔG_{cov}). Data points represent individual mutants, revealing a positive correlation (Pearson's r = 0.67). **c,** Surface mapping of energetic contributions to non-covalent binding. Residues are colored according to the change in non-covalent binding free energy ($\Delta\Delta G_{\text{non-cov}}$) upon alanine substitution, mapped onto the crystal structure of SfbI-TED (PDB 5A0L). Mutation of H93 (loop 1) abolished binding, identifying it as a key hotspot. L112, Y115, and R118 (loop 2) also contributed significantly, whereas loop 3 showed a negligible contribution. **d,** Representative BLI sensorgrams for wild-type SfbI-TED and selected mutants (L112T and F116Y). The plots display the kinetic sequence consisting of (i)-(iv) association and dissociation steps at pH 7.3 across a fibrinogen concentrations of 25, 100, 400, and 1600 nM, respectively, (v) a dissociation step at pH 6.0, (vi) two wash cycles in pH 2.0 buffer where all non-covalent interactions are dissociated, and (vii) the final response at pH 7.3, corresponding to the fraction of covalently crosslinked complex formed.

Evidence for conserved pH-responsive behavior within the TED family

Finally, we assessed whether pH responsiveness is unique to SfbI-TED or is shared more broadly among TEDs. To address this, we examined the TEDs from two additional proteins: CpTIE-TED from *Clostridium perfringens* and FbaB-TED from GAS. For CpTIE-TED, the pH-dependent cleavage of the intramolecular thioester bond was measured using the same 4-PDS assay employed for SfbI-TED. Given that the only thiol-containing residue in CpTIE-TED is cysteine involved in the thioester bond, all detected thiols directly reflect bond cleavage. Consistent with SfbI-TED, CpTIE-TED displayed a clear pH dependence of thioester bond cleavage (Fig. 5a).

FbaB is a surface protein encoded in the same FCT region of the GAS genome as SfbI[18]. FbaB-TED also binds fibrinogen and possesses a C-terminal fibronectin-binding repeat region, rendering it similar to SfbI[15]. Although FbaB is therefore not ideal for probing the evolutionary conservation of pH responsiveness across distantly related TEDs, it is, alongside SfbI, one of only two TEDs for which a physiological target has been identified. This renders it suitable for testing pH-dependent target binding. Using BLI, we found that FbaB-TED complexes with fibrinogen dissociated rapidly at pH 6.0 (Fig. 5b).

The sequence identity between CpTIE-TED and SfbI-TED was only 26%, while that between FbaB-TED and SfbI-TED was 25%, with most of the conserved positions confined to the buried core (Fig. 5c,d). The observation of consistent pH responsiveness despite such low sequence identity suggests that this behavior arises from features intrinsic to the TED fold rather than from sequence-specific determinants.

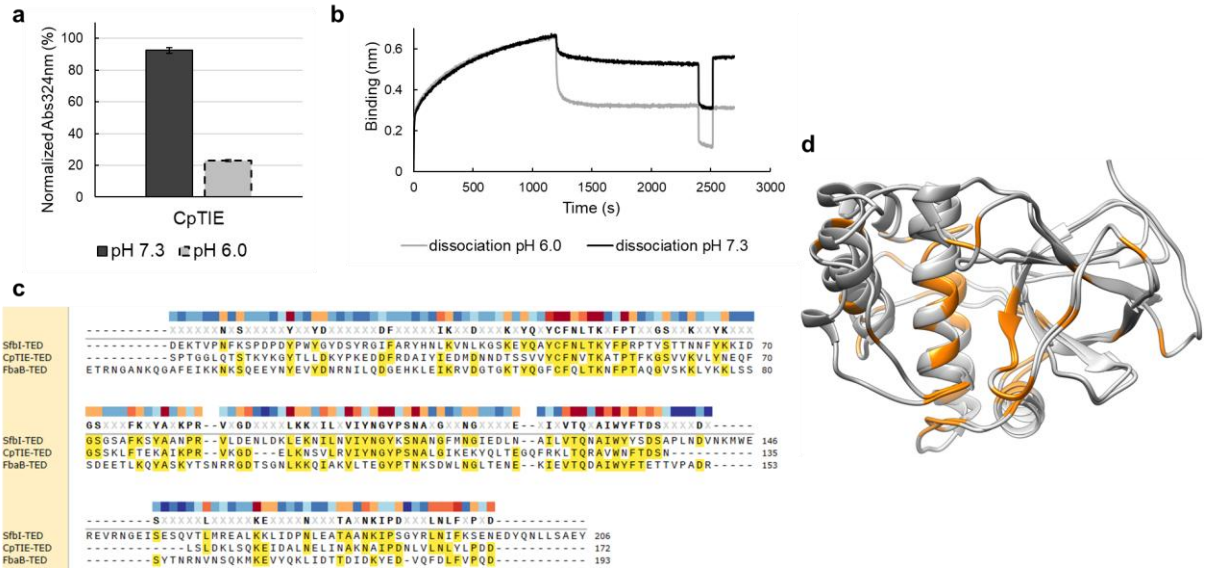

Fig. 5 | pH responsiveness in other TEDs.
a, pH-dependent reactivity of the intramolecular thioester bond in CpTIE-TED from *C. perfringens*. **b,** BLI analysis of fibrinogen binding by FbaB-TED from GAS. The sensorgrams display kinetic phases consisting of association at pH 7.3, followed by dissociation in wash buffers at either pH 7.3 or pH 6.0, confirming that rapid acid-induced dissociation is a conserved feature. **c,** Sequence conservation among TEDs. Pairwise sequence identities of CpTIE-TED and FbaB-TED relative to SfbI-TED are 26% and 25%, respectively. Residues conserved across two or three sequences are highlighted in yellow. The heat map above the alignment indicates conservation scores calculated by the Valdar method and visualized using SnapGene Viewer. **d,** Structural alignment of SfbI-TED (PDB 5A0L) and CpTIE-TED (PDB 5A0G). Residues identical in sequence are colored orange.

Discussion

In this study, we demonstrated that the interaction between SfbI-TED and fibrinogen is a reversible two-step process comprising of non-covalent recognition followed by intermolecular isopeptide bond formation, with the latter being pH-dependent. In this section, we demonstrate that this pH responsiveness is rooted in the intrinsic pH dependence of thioester chemistry that is conserved across the TED family. We then evaluated the possibility that pH responsiveness is a property feature of TED domains and proposed a new hypothesis regarding the physiological function of TEDs, which serve as adhesins widely distributed among Gram-positive bacteria.

To formalize the pH dependence of the reaction free energy, we employed Alberty's framework of transformed Gibbs energies, defined at a fixed pH, with all other species in their standard states[31]. Within this framework, the reaction free energy can be expressed as the sum of a pH-independent term ($\Delta_r G^\circ$) and a pH-dependent term (Fig. 6a). Accordingly, changes in the reaction free energy upon a pH shift are fully captured by the latter term, such that only $\Delta\Delta_r G'^\circ(\text{pH } 6.0 \rightarrow 7.3)$ needs to be considered. $\Delta\Delta_r G'^\circ$ can be further decomposed into two contributions (Fig. 6b). One term, $\Delta\Delta_r G'^\circ_{\text{acyl-transfer}}$, arises from protonation equilibria of the functional groups directly involved in the thioester reaction, namely the thioester bond itself and the nucleophile. The second term, $\Delta\Delta_r G'^\circ_{\text{other}}$ encompasses all remaining contributions, including changes in the pK_a values of general acid–base catalytic residues surrounding the thioester bond. Crucially, the former contribution can be explicitly calculated within Alberty's framework. Detailed theoretical discussions are provided in the Supplementary Note.

First, we analyzed the pH-dependent reaction free energy of the intramolecular thioester bond cleavage. A plausible mechanism for this cleavage reaction is hydrolysis, wherein new titratable groups emerge as the reaction proceeds:

$$\text{R}_1\text{-CO-S-R}_2 + \text{H}_2\text{O} \rightleftharpoons \text{R}_1\text{-COOH} + \text{R}_2\text{-SH}$$

For this cleavage reaction, the theoretical value of $\Delta\Delta_r G'^{\circ}_{\text{acyl-transfer}}(\text{pH } 6.0\rightarrow 7.3)$ is -1.77 (kcal/mol) (Eq. S6). This value can be perturbed as a function of the pK_a of the carboxyl group (R1-COOH) and the thiol group (R2-SH) and it is derived using typical solution values[32].

Meanwhile, the pH responsiveness of the reaction can be experimentally determined to be $\Delta\Delta_r G'^{\circ}(\text{pH } 6.0\rightarrow 7.3) = -1.63 \pm 0.24$ (kcal/mol) (mean $\pm$ SD, n=3), using the normalized A_{324} values to estimate the equilibrium constant (Eq. S7-8). From the difference between the experimentally determined $\Delta\Delta_r G'^{\circ}(\text{pH } 6.0\rightarrow 7.3)$ and the theoretically calculated $\Delta\Delta_r G'^{\circ}_{\text{acyl-transfer}}(\text{pH } 6.0\rightarrow 7.3)$, we obtain $\Delta\Delta_r G'^{\circ}_{\text{other}}(\text{pH } 6.0\rightarrow 7.3) = +0.14 \pm 0.24$ (kcal/mol) (Eq. S9). This result indicates that most of the macromolecular-level pH responsiveness of SfbI-TED originates from the acyl transfer reaction itself, with only minor contributions from the surrounding protein environment. Visual inspection of the region surrounding the thioester bond in the 3D structure of SfbI-TED did not reveal functional groups poised to act as general acid–base catalysts. Consistent with this observation, sequence conservation analysis across the Pfam-annotated TED family (PF08341) showed no conserved residues of this type near the thioester bond (Fig. S9).

In the above analysis, we assumed that the cleavage detected by the thiol quantification assay primarily reflected the hydrolysis of the intramolecular thioester bond. Nevertheless, even in the absence of low-molecular-weight amines, aminolysis mediated by intrinsic amino groups of SfbI-TED cannot be entirely excluded. Importantly, even under these circumstances, our thermodynamic conclusions remain robust (Eqs. S10–15).

Having established the general principles of TED reactivity, we now turn to the reaction of primary physiological relevance: the formation and cleavage of the intermolecular isopeptide crosslink with the target protein. This reaction can be readily explained using the same thermodynamic framework.

$$\mathrm{R_1\text{-}CO\text{-}S\text{-}R_2 + R_3\text{-}NH_2 \rightleftharpoons R_1\text{-}CO\text{-}NH\text{-}R_3 + R_2\text{-}SH}$$

For this reaction as well, the theoretical value of $\Delta\Delta_{\mathrm{r}}G'^{\circ}_{\text{acyl-transfer}}(\text{pH } 6.0\rightarrow 7.3)$ is $-1.77\ (\mathrm{kcal/mol})$, considering only the three residues that are directly involved in the acyl-transfer reaction; the pH responsiveness at the macromolecular level can be rationalized by additionally incorporating $\Delta\Delta G'^{\circ}_{\text{other}}$ (Eq. S17–18). As in the case of intramolecular thioester bond cleavage, the contribution of $\Delta\Delta G'^{\circ}_{\text{other}}$ is unlikely to be sufficient to appreciably counterbalance the pH dependence dictated by $\Delta\Delta_{\mathrm{r}}G'^{\circ}_{\text{acyl-transfer}}$ in the intermolecular reaction either. As an order-of-magnitude estimate, assuming that pK_{a} shifts within the complex arising from acyl-transfer are negligible, the reaction free energy for intermolecular crosslink formation is −1.21 kcal/mol (favorable) at pH 7.3, whereas it shifts to +0.57 kcal/mol (unfavorable) at pH 6.0, as calculated based on FASTIA results (Fig. 4b). This confirms a switch in thermodynamic favorability across this pH range (Fig. 6c).

Notably, these considerations are solely from an equilibrium perspective, which alone does not guarantee that the reaction will proceed at an appreciable rate. However, BLI kinetic analysis demonstrated that acidification accelerates dissociation (Fig. 3b). Overall, while the SfbI-TED–fibrinogen complex remains stable near neutral pH, it dissociates at a biologically relevant rate in response to environmental acidification.

Next, we investigated whether pH-responsive binding is conserved across the TED family. Since the conserved acyl transfer reaction itself intrinsically exhibits pH responsiveness, this regulation likely represents a general feature of TEDs. Notably, however, the reaction free energy comprises of a pH-independent term ($\Delta_{\mathrm{r}}G^{\circ}$) and a pH-dependent term (Fig. 6a); whether this intrinsic pH responsiveness manifests at the macromolecular level depends on the balance between these two contributions.

For example, increasing the instability of the thioester bond promotes intermolecular crosslinking. Independently, strengthening the target-specific non-covalent interactions further facilitates this crosslinking

(Fig. 4b). Under such conditions, the contribution of the pH-independent term ($\Delta_r G°$) dominates, requiring more acidic conditions for efficient cleavage reaction(Fig. 6d); consequently, the pH-responsive component may be effectively masked within the physiologically relevant pH range, precluding a detectable shift. Indeed, in the SfbI-TED L112T mutant, the fibrinogen complex remained stable across the tested pH range.

Notably, CpTIE-TED exhibits pH responsiveness despite its distant sequence and taxonomic relationship to SfbI-TED. Thiol quantification confirmed that the thermodynamic favorability of the CpTIE-TED reaction switches between pH 6.0 and 7.3 (Fig. 5a). Similarly, although the trait of near-irreversible binding to fibrinogen is accessible through a single L112T mutation, SfbI-TED likely avoided this course of evolution. These findings strengthen the hypothesis proposed by Echelman *et al.* that reversible adhesion confers an advantage to bacteria[19,20]. Furthermore, excessive instability of the intramolecular thioester bond hinders efficient repair following cleavage by the abundant amines present *in vivo*[30]. Taken together, these observations support the generalization that, in principle, pH-responsive adhesion represents an intrinsic property shared across the TED family, although this property may obscure this trait in some evolved TEDs.

Previous studies postulated that TEDs might function as molecular anchors that irreversibly tether bacteria to host tissues. In contrast, our results demonstrate that SfbI-TED binding is reversible, with a lifetime comparable to other adhesins. This raises a fundamental question: What biological advantage does covalent adhesion provide? While Echelman *et al.* proposed that mechanical force modulates “smart covalent bond” lifetimes, we proposed a distinct but complementary perspective: TEDs have proliferated because they act as versatile, mechanism-based, pH-responsive adhesion modules. In GAS, for example, fibrinogen binding is reported to sterically inhibit host phagocytosis[33], yet this same coating impairs the function of other adhesins[34]. Consequently, SfbI’s ability to switch fibrinogen binding on and off in a pH-responsive manner confers a strategic advantage.

Conventional pH-responsive binders typically rely on interface residues whose protonation states vary with pH[35]. In contrast, the thioester bond embedded within the structural core intrinsically confers pH responsiveness to TEDs. Consequently, TEDs retain pH-dependent binding regardless of the target-recognition interface diversity or target surface properties, provided the reaction utilizes thioester chemistry. We proposed that this modular ability to implement pH-responsive binding via a conserved catalytic motif, without constraining the evolving binding interface, underlies the widespread distribution and evolutionary success of TEDs across Gram-positive bacteria.

Research on bacterial adaptation to environmental pH has traditionally focused on pH-dependent gene expression. Although such transcriptional regulation drives infection dynamics and virulence, the pH modulation of protein function warrants equal consideration, as these mechanisms enable adaptive responses on different timescales. By characterizing isolated TEDs independent of species-specific regulation, we revealed that this broadly distributed adhesin family functions as an intrinsically pH-responsive adhesion module. Integrating pH-dependent binding modulation into the emerging physiological analyses of TED family members is essential for elucidating their full biological roles.

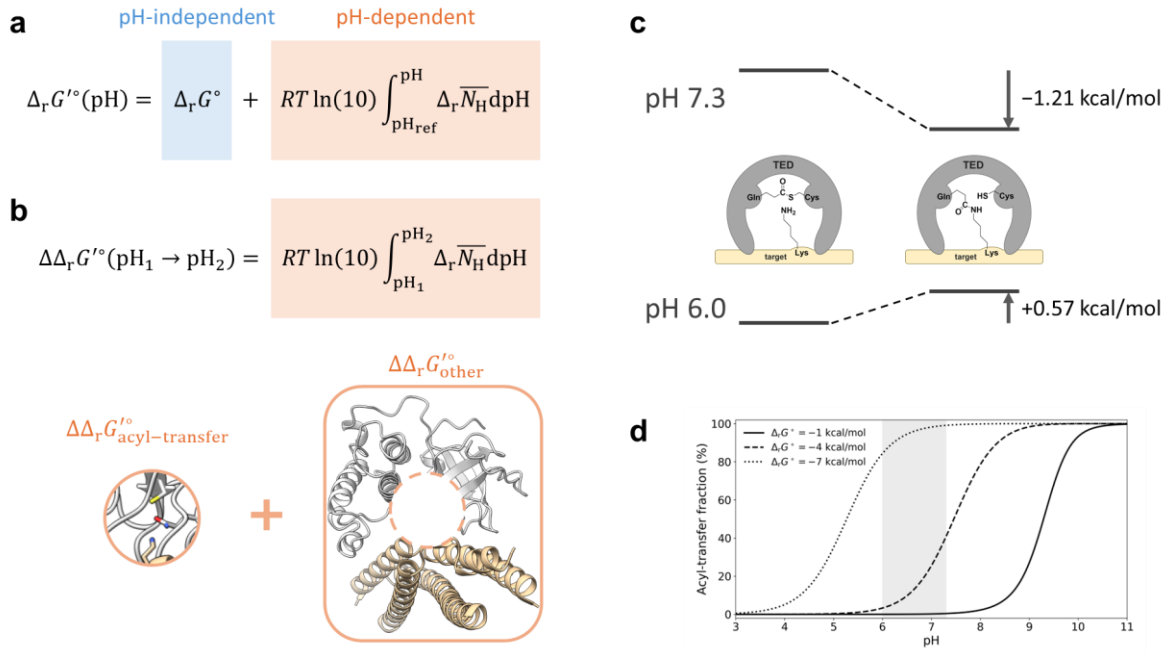

Fig. 6 | Graphical representation of the thermodynamic analysis of pH responsiveness. **a,** Decomposition of transformed standard reaction free energy into pH-independent and pH-dependent terms according to Alberty's framework. $\Delta_r\overline{N_H}$ denotes the change in the average number of bound protons accompanying the reaction. **b,** Decomposition of the pH-dependent change in the transformed standard reaction free energy into two contributions: one arising from the reactive triad, comprising the thioester-forming cysteine and glutamine as well as the target lysine, and the other encompassing all remaining factors. Structure adapted from Fig. 4a. **c,** Thermodynamic switching of reaction favorability in the intermolecular isopeptide bond formation. **d,** Effect of the pH-independent term on the manifestation of intrinsic pH responsiveness of the acyl-transfer reaction at the macromolecular level.

Methods

Protein expression in *Escherichia coli*

With the exception of the mutants analyzed by FASTIA, all TEDs and SpyCatcher003[36,37] used in this study were expressed in *E. coli* BL21(DE3). Expression vectors were derived from pCold II (Takara Bio) for cytoplasmic expression. Wild-type and mutant SfbI-TED constructs contained N-terminal 6xHis-SpyTag003 tags. FbaB-TED was similarly tagged at the C-terminus. CpTIE-TED was tagged N-terminally with a 6xHis-SUMO. SpyCatcher003 was produced with either an N-terminal 6xHis alone or combined with C-terminal AviTag.

Plasmids were transformed into BL21(DE3) cells, and plated on LB agar containing 100 μg/mL ampicillin. Colonies were inoculated into 6 mL of LB broth containing 100 μg/mL ampicillin and cultured overnight at 37 °C with shaking at 200 rpm. The seed culture was then transferred to 800 mL of LB broth containing 100 μg/mL ampicillin in baffled flasks, which were incubated at 37 °C with shaking at 120 rpm. When the optical density at 600 nm (OD_{600}) reached 0.4, the culture was cooled at 4 °C for 30 min. Protein expression was induced with 0.5 mM isopropyl β-D-1-thiogalactopyranoside (IPTG), followed by overnight incubation at 15 °C. Finally, cells were harvested by centrifugation (8,000 × g for 10 min) and the pellets stored till further processing.

Purification by immobilized metal affinity chromatography (IMAC)

The cell pellet was resuspended in 30 mL of lysis buffer (20 mM Tris-HCl, 500 mM NaCl, and 5 mM imidazole, pH 8.0) and lysed by sonication on ice for 15 min. The lysate was clarified by centrifugation (40,000 × g for 1 h), and the supernatant was filtered (0.2-μm filter) before loading onto a gravity-flow column (15 mm diameter, Bio-Rad) packed with Ni-NTA agarose resin (QIAGEN). All subsequent steps were performed at 4 °C. The resin was washed with 15 column volumes (CV) of wash buffer (20 mM Tris-HCl, 500 mM NaCl, and 20 mM imidazole, pH 8.0). Finally, proteins were eluted with 5 CV elution buffer

(20 mM Tris-HCl, 500 mM NaCl, and 200 mM imidazole, pH 8.0).

To remove the N-terminal 6xHis-SUMO tag from CpTIE-TED, the IMAC eluate was incubated overnight at 4 °C with in-house-produced Ulp1 protease while dialyzing against 50 volumes of cleavage buffer (20 mM Tris-HCl, 150 mM NaCl, pH 8.0). Following digestion, the imidazole concentration was adjusted to 5 mM, and the sample was incubated with the Ni-NTA resin for 1 h with gentle rotation. The mixture was then applied to an empty gravity-flow column, and the flow-through containing untagged CpTIE-TED was collected.

Size-exclusion chromatography (SEC)

The IMAC eluate (or the flow-through fraction for CpTIE-TED) was dialyzed overnight against 50 volumes of SEC buffer (20 mM HEPES-NaOH, 150 mM NaCl, pH 7.3). The protein was further purified via SEC on a HiLoad 26/600 Superdex 75 pg column (Cytiva) connected to an ÄKTA prime system equilibrated with SEC buffer. Fractions containing monomeric protein were pooled for subsequent experiments.

Buffer exchange for biochemical and biophysical analyses

SEC-purified proteins obtained at pH 7.3 were used directly for experiments performed at that pH. For other pH levels, proteins were dialyzed into the following target buffer systems: 20 mM HEPES-NaOH and 150 mM NaCl for pH 7.0 and 8.0, or 20 mM Bis-Tris-HCl and 150 mM NaCl for pH 6.0 and 6.5. For CD spectroscopy, proteins were exchanged into PBS (pH 7.4) to minimize background absorbance in the far-UV region (< 200 nm). Standard dialysis involved 50 volumes of the target buffer overnight at 4 °C. For DSC measurements, a rigorous two-step dialysis was conducted: initial dialysis for 4 h against 50 volumes of buffer, followed by overnight dialysis against fresh buffer. Protein concentrations were determined by measuring the absorbance at 280 nm (A_{280}) using a NanoDrop One spectrophotometer (Thermo Fisher Scientific) and adjusted for each experiment.

Differential scanning calorimetry (DSC)

Wild-type SfbI-TED was analyzed across five pH conditions (6.0, 6.5, 7.0, 7.5, and 8.0), whereas the C109A, C109S, and Q261A mutants were analyzed at pH 6.0 and 7.5. All samples were prepared at a concentration of 20 μM.

DSC measurements were performed using a MicroCal PEAQ-DSC automated system (Malvern Panalytical). Thermal scans were conducted from 20 °C to 110 °C at a scan rate of 1 °C/min. The data within the 30–80 °C range, which encompassed the observed thermal transitions, were utilized for analysis. Buffer baselines were subtracted, and the resulting thermograms were fitted to the Non-Two-State model using the MicroCal PEAQ-DSC Software (version 1.40).

Circular dichroism (CD) spectroscopy

Far-UV CD spectra of wild-type SfbI-TED and the C109A and Q261A mutants were recorded at 25 °C (pH 6.0 and 7.4) using a J-1500 spectropolarimeter (JASCO). Samples (5 μM) were measured in a 1-mm path length quartz cuvette. Spectra were obtained by scanning from 260 to 200 nm at 60 nm/min, with five accumulations averaged per sample. Following buffer-baseline subtraction from the raw data, the corrected spectra were converted to molar ellipticity based on the protein concentration and path length.

Thiol quantification upon thermal denaturation

Free thiol content was quantified using 4,4′-dithiodipyridine (4-PDS). A 100 mM stock solution of 4-PDS was prepared in methanol. Protein samples (SfbI-TED or CpTIE-TED) were prepared in either pH 7.3 buffer (20 mM HEPES-NaOH, 150 mM NaCl) or pH 6.0 buffer (20 mM Bis-Tris-HCl, 150 mM NaCl). The protein solutions and 4-PDS stock were equilibrated to room temperature and mixed to yield final concentrations of 30 μM protein and 100 μM 4-PDS, respectively, in a 200 μL volume. Control samples contained 100 μM 4-

PDS in each corresponding buffer without the addition of protein.

Immediately after mixing, samples were transferred to a thermal cycler (MiniAmp Plus, Thermo Fisher Scientific), and subjected to the following thermal profile: heating from 25 °C to 75 °C at a ramp rate of 3.5 °C/s, holding at 75 °C for 30 s, cooling to 2 °C at a rate of 3.5 °C/s, and holding at 2 °C for 2 min. Following this treatment, all protein samples (wild-type SfbI-TED, mutants, and CpTIE-TED) exhibited visible turbidity. Aggregates were removed via filtration through 0.2-µm centrifugal devices (Nanosep, Pall Corporation) at 5,000 rpm for 1 min. The resulting filtrates were immediately analyzed by UV–visible spectroscopy.

Absorbance spectra were recorded from 400 to 240 nm using a V-660 spectrophotometer (JASCO) equipped with a water-cooled Peltier cell changer (PAC-743). An empty cuvette served as the baseline. To account for background absorbance and potential thermal degradation of 4-PDS, the spectrum of the protein-free control was subtracted from the corresponding protein-containing sample. Normalized absorbance at 324 nm (A_{324}) was calculated as follows:

$$\text{Normalized } A_{324}\ (\%) = \frac{A_{324}}{\varepsilon_{324} \times C_{\text{protein}} \times l} \times 100$$

where ε_{324} is the extinction coefficient of 4-thiopyridone (4-TP) at 324 nm (21,400 M^{-1} cm^{-1}, determined experimentally from its reaction with cysteine in a previous study[25]), C_{protein} is the molar concentration of the protein (30 µM), and l is the path length (1 cm).

Reactivity of SfbI-TED with 4-PDS under native conditions

To monitor thioester-bond cleavage in folded SfbI-TED, 30 µM SfbI-TED (wild type or Q261A) was incubated with 100 µM 4-PDS in pH 7.3 buffer (20 mM HEPES-NaOH, 150 mM NaCl) or pH 6.0 buffer (20 mM Bis-Tris-HCl, 150 mM NaCl). A_{324} was recorded every 10 s for up to 24 h at room temperature. To exclude a direct reaction between 4-PDS and the thioester moiety, control reactions utilized 30 µM

acetylthiocholine iodide as a small-molecule thioester model. Background absorbance changes were assessed by monitoring 100 μM 4-PDS in the respective buffers without protein or thioester compounds.

Identification of peptides after thioester hydrolysis by nanoLC-MS/MS

SfbI-TED samples (pH 7.3) were mixed (1:3 volume ratio) with an SDS-PAGE loading buffer lacking amines and reducing agents (50 mM HEPES-NaOH, 18.4 g/L SDS, 4.5% glycerol, 0.013 g/L bromophenol blue, pH 7.3) and incubated at room temperature for 10 min. Samples were separated by SDS-PAGE in running buffer (3 g/L Tris, 14.4 g/L glycine, and 1 g/L SDS) at 200 V for 60 min. Following Coomassie Brilliant Blue staining, protein bands were excised, destained, and subjected to in-gel digestion with trypsin at 37 °C for 16 h. Proteome analysis was performed by Orbitrap Eclipse Tribrid mass spectrometer with a FAIMS Pro interface (Thermo Fisher Scientific, Waltham, MA) coupled to Vanquish Neo UHPLC system (Thermo Fisher Scientific, Waltham, MA). The peptides were separated on a reversed-phase column using a linear gradient of 2–24% acetonitrile in 0.1% formic acid at a flow rate of 300 nL/min. Full MS scans were acquired in the Orbitrap at a resolution of 120,000, followed by MS/MS scans in the ion trap using higher-energy collisional dissociation (HCD) with a normalized collision energy of 35% and a maximum injection time of 10 ms. Peptide identification was carried out by searching against the customized database derived from UniProt human reference proteome (UP000005640) supplemented with the amino acid sequence of SfbI-TED using the Sequest HT algorithm in Proteome Discoverer Software (version 2.5) (Thermo Fisher Scientific, Waltham, MA, USA).

Biotinylation of SpyCatcher003

Purified SpyCatcher003 fused with an N-terminal 6xHis and a C-terminal AviTag (SpyCatcher003-His-Avi) was dialyzed overnight against 20 mM Tris-HCl and 50 mM NaCl at pH 8.0. Biotinylation was performed in a 500-μL reaction mixture containing 28 μM SpyCatcher003-His-Avi, 0.1 mg/mL BirA ligase, 50 mM Bicine, 10 mM $MgSO_4$, 10 mM ATP, and 50 μM D-biotin. The mixture was then incubated at 30 °C for

60 min. The reaction mixture was subsequently buffer-exchanged into 20 mM HEPES-NaOH and 150 mM NaCl (pH 7.3) using a PD-MiniTrap G-25 column (Cytiva).

Bio-layer interferometry (BLI)

Bio-layer interferometry measurements were performed using an Octet RED384 system (Sartorius). All assays were conducted at 30 °C with plate agitation at 1,000 rpm. Unless otherwise specified, the running buffer contained 20 mM HEPES-NaOH, 150 mM NaCl, and 0.05% (v/v) Tween-20.

Assay 1: pH-dependent binding analysis (Fig. 3)

SAX2 biosensors (Sartorius) were hydrated for 10 min and loaded with 2 μM biotinylated SpyCatcher003-His-Avi for 5 min. To remove loosely bound proteins, the biosensors were regenerated using 10 mM glycine (pH 2.0). SfbI-TED (10 μM; wild type, C109A, or Q261A) was then captured for 20 min via the SpyTag003–SpyCatcher003 reaction[38]. Following capture, a second wash with 10 mM glycine (pH 2.0) was performed. The establishment of a stable baseline after this wash confirmed the removal of unreacted SfbI-TED and formation of a covalent complex.

Analyte solutions were prepared by dissolving human fibrinogen (Sigma-Aldrich) in running buffer and filtering through a 0.2-μm Nanosep centrifugal device (Pall Corporation). The fibrinogen concentration was determined via A_{280}. Association kinetics were measured by dipping the TED-immobilized biosensors into 100 nM fibrinogen, followed by dissociation in running buffer at the indicated pH values (pH 6.0 and 7.3 for Fig. 3a; pH 5.0, 5.5, 6.0, 6.5, 7.3, and 8.0 for Fig. 3b). After each dissociation, biosensors were regenerated with 10 mM glycine (pH 2.0) and re-equilibrated in running buffer. The C109A mutant exhibited no detectable binding to fibrinogen and showed lower nonspecific adsorption than SpyCatcher003-only biosensors; therefore, the C109A signal subtracted as a reference from the wild type and Q261A data.

Assay 2: Covalent crosslinking analysis (Fig. 5b and Extended Data Fig. 4)

SpyCatcher003 fused with an N-terminal 6xHis (10 μM) was diluted 20-fold into 10 mM sodium acetate (pH 4.5) and immobilized onto AR2G biosensors (Sartorius) pre-activated with EDC/sulfo-NHS for 2 min. Unreacted esters were quenched with 1 M ethanolamine (pH 8.3). FbaB-TED or SfbI-TED (wild type or Q261A; 20 μM) was captured via the SpyTag003–SpyCatcher003 reaction for 30 min, followed by regeneration with 10 mM glycine (pH 2.0).

Fibrinogen was prepared as described above and used at a concentration of 5 μM. The biosensors were exposed to fibrinogen and subsequently processed under one of the following conditions to assess intermolecular crosslinking: (i) washing at pH 6.0, (ii) washing at pH 7.3, (iii) direct regeneration with 10 mM glycine (pH 2.0) without dissociation, or (iv) regeneration with 10 mM glycine (pH 2.0) after dissociation. For the experiments shown in Extended Data Fig. 4, biosensors were re-incubated with 5 μM fibrinogen following the dissociation at pH 6.0 to confirm fibrinogen-binding capacity was retained.

Complex structure prediction by AlphaFold 3

Fibrinogen is a hexamer composed of two sets of Aα, Bβ, and γ chains (PDB 3GHG)[39]. For complex modeling, the sequences corresponding to the coiled-coil region of the fibrinogen heterotrimer were used, focusing on the region containing Lys100 of the Aα chain, which was previously identified as the SfbI-TED binding site[15].

Structure prediction was performed using the AlphaFold 3. Calculations were performed using 100 random seeds to sample the conformational space extensively and generate 500 predicted complex structures. For each model, the distance was calculated between the carbonyl carbon of the SfbI-TED thioester and the ε-amino nitrogen (NZ) of lysine residues on fibrinogen. Lysine residues with an interatomic distance of less than 5 Å were defined as being positioned for recognition by TED. The model exhibiting the shortest

nucleophile–electrophile distance was selected for visualization.

High-throughput mutational analysis using FASTIA

High-throughput mutational scanning was performed using the FASTIA platform[28]. A pET28b-based plasmid encoding SfbI-TED fused to the N-terminal 6xHis-SpyTag003 served as a template for generating individual SfbI-TED mutants. Single mutations were introduced into the residues within the putative fibrinogen-binding interface, as predicted by AlphaFold 3.

Linear DNA fragments encoding each mutant were generated by inverse polymerase chain reaction (PCR) using KOD One DNA polymerase (TOYOBO) and mutagenic primers. The template plasmid was removed by DpnI digestion and the PCR products were purified using a NucleoSpin 8 PCR Clean-up kit (MACHEREY-NAGEL). The fragments were circularized using the NEBuilder HiFi DNA Assembly Kit (New England Biolabs). The resulting circular DNA was used as a template for a second PCR amplification with the primers PURExfrex-F and PURExfrex-R to generate linear expression templates containing the T7 promoter, ribosome-binding site, 6xHis, SpyTag003, and the SfbI-TED coding region. These linear DNA fragments were purified and sequenced by Sanger sequencing (Fasmac).

Cell-free protein synthesis was carried out using the PURExfrex 2.1 system (GeneFrontier). Reaction mixtures (10 μL) were supplemented with 4 mM reduced glutathione, 3 mM oxidized glutathione, 5 μM DnaK, 1 μM DnaJ, 1 μM GrpE, 1 μM DsbC, and 5 ng of template DNA. Reaction mixtures were incubated at 37 °C for 16 h. Following synthesis, the mixtures were diluted eight-fold in running buffer (20 mM HEPES-NaOH, 150 mM NaCl, 0.05% (v/v) Tween-20, pH 7.3) supplemented with 20 mM $MgCl_2$ to stabilize ribosomes and used directly for BLI immobilization.

Interaction kinetics were analyzed using BLI on the SAX2 biosensors. SpyCatcher003-His-Avi was used

without *in vitro* biotinylation, relying on partial biotinylation by endogenous ligases during expression in *E. coli*[40]. This allowed immobilization at higher SpyCatcher003 concentrations than in the purified assay, yielding loading responses of approximately 0.5–0.6 nm. The immobilization protocol was identical to that described above, except that an acidic wash (10 mM glycine-HCl, pH 2.0) was omitted after capturing SfbI-TED through the SpyCatcher003-SpyTag003 reaction to prevent the denaturation of potentially unstable mutants. Stable baselines confirmed that most of the SfbI-TED mutants were successfully immobilized.

Kinetic parameters were determined using single-cycle kinetics. The biosensors were sequentially dipped into four increasing concentrations of fibrinogen (25, 100, 400, and 1600 nM) for 120 s in running buffer. Each association step was followed by a dissociation step in the running buffer for 120 s. After the final association step at 1600 nM, the dissociation was monitored for 10 min. Finally, the biosensors were transferred to dissociation buffer adjusted to pH 6.0, to assess the dissociation kinetics under acidic conditions. Measurements were performed in triplicate.

Curve fitting for FASTIA mutant analysis

Equilibrium constants for the non-covalent interaction and intermolecular crosslinking were determined by fitting the series of association and dissociation curves at pH 7.3 to the two-step reaction model described in the main text. The parameter vector $\boldsymbol{p}$ was defined as follows:

$$\boldsymbol{p} = (k_{\mathrm{on}}, k_{\mathrm{off}}, k_{\mathrm{c}}, k_{\mathrm{c,rev}}, R_{\mathrm{max}})^{\mathrm{T}}$$

For each time point $t = t_i$, the residual r_i was calculated as the difference between the measured response $R(t_i)$ and model response $R_{\mathrm{model}}(t_i; \boldsymbol{p})$:

$$r_i = R(t_i) - R_{model}(t_i;\ \boldsymbol{p})$$

The residual vector $\boldsymbol{r}$ was defined as:

$$\boldsymbol{r} = (r_1, r_2, , , r_N,)^{\mathrm{T}}$$

where N denotes the total number of data points in the time series recorded at 1 s intervals.

Parameter optimization was performed using the Trust Region Reflective algorithm implemented in the scipy.optimize.least_squares function (SciPy library) [41] to minimize the squared Euclidean norm of $\boldsymbol{r}$. Based on the optimized parameters, the equilibrium constants were calculated as:

$$K_{\text{non-cov}} = \frac{k_{\text{on}}}{k_{\text{off}}}$$

$$K_{\text{cov}} = \frac{k_{\text{c}}}{k_{\text{c,rev}}}$$

The corresponding reaction free energies, $\Delta G_{\text{non-cov}}$ and ΔG_{cov}, were calculated using the standard thermodynamic relationship:

$$\Delta G = -RT \ln K$$

Evaluation of parameter reliability

Since all fitting parameters—including those subsequently used to calculate $\Delta G_{\text{non-cov}}$ and ΔG_{cov}—were estimated simultaneously from a single sensorgram, a rigorous evaluation of parameter standard errors and identifiability was essential.

To evaluate the reliability of the derived free energies, we performed error-propagation analysis. After the optimization of the parameter vector $\boldsymbol{p}$, the Jacobian matrix $\boldsymbol{J}$ (N × P) was calculated as:

$$\boldsymbol{J}_{ij} = \frac{\partial r_i}{\partial p_j}$$

The parameter covariance matrix $\boldsymbol{C}_p$ was estimated as:

$$\boldsymbol{C}_{\mathbf{p}} = s^2 (\boldsymbol{J}^T \boldsymbol{J})^{-1}$$

where s^2 is the noise variance estimate calculated from the residual sum of squares:

$$s^2 = \frac{1}{N-P} \sum_{i=1}^{N} r_i^2$$

Here, N = 1,440 represents the total number of data points in the 1,440-second sensorgram (recorded at 1-s intervals), and P = 5 is the number of optimized parameters.

Next, the covariance matrix of the equilibrium constants ($\boldsymbol{C_K}$) was estimated by linear error propagation using the Jacobian of the equilibrium constants with respect to $\boldsymbol{p}$ ($\boldsymbol{J_K}$) as follows:

$$\boldsymbol{J_K} = \frac{\partial K_i}{\partial p_j}, \boldsymbol{C_K} = \boldsymbol{J}_K \boldsymbol{C_p} \boldsymbol{J}_K^T$$

Similarly, the covariance matrix of the reaction free energies ($\boldsymbol{C_{\Delta G}}$) was derived using the Jacobian of the free energies with respect to the equilibrium constants ($\boldsymbol{J_{\Delta G}}$):

$$\boldsymbol{J_{\Delta G}} = \frac{\partial \Delta G_i}{\partial K_j}, \boldsymbol{C_{\Delta G}} = \boldsymbol{J}_{\Delta G} \boldsymbol{C}_K \boldsymbol{J}_{\Delta G}^T$$

The standard errors of each ΔG were taken as the square roots of the diagonal elements of $\boldsymbol{C_{\Delta G}}$. Fits were accepted only if they satisfied the criterion:

$$\text{S.E.}(\Delta G_i)/|\Delta G_i| < 15\%$$

To further exclude fits where $\Delta G_{\text{non-cov}}$ and ΔG_{cov} were not independently identifiable, we applied the Motulsky and Christopoulos criterion[42], requiring that the magnitude of the error-correlation coefficient $\rho_{\Delta G}$ must not exceed 0.9:

$$|\rho_{\Delta G}| = \left| \frac{\text{cov}(\Delta G_{\text{non-cov}}, \Delta G_{\text{cov}})}{\text{S.E.}(\Delta G_{\text{non-cov}}) \cdot \text{S.E.}(\Delta G_{\text{cov}})} \right| > 0.9$$

where $\text{cov}(\Delta G_{\text{non-cov}}, \Delta G_{\text{cov}})$ is the off-diagonal element of the 2 × 2 matrix $\boldsymbol{C_{\Delta G}}$.

Only the fits satisfying both the relative standard error and correlation criteria were used for the final analysis. For each mutant, the mean values of $\Delta G_{\text{non-cov}}$ and ΔG_{cov} were calculated from the accepted fits. The Pearson correlation coefficient across mutants was determined to investigate the relationship between non-covalent interactions and intermolecular crosslinking reactions.

Acknowledgements

We are grateful to GeneFrontier Corporation for providing the PURExpress components. This work was supported by the Japan Agency for Medical Research and Development (AMED) under grant numbers JP223fa627001 (UTOPIA), JP223fa727002 (SCARDA), and JP24ama121033 (BINDS) to K. T.; JSPS KAKENHI under grant number 22K21343 to K. T.; and JST ACT-X under grant number JP JPMJAX222I to R. M. We would like to thank Editage (www.editage.jp) for English language editing.

1 **Reference**

2 1. Ayazi, S. *et al.* A new technique for measurement of pharyngeal pH: normal values and discriminating

3 pH threshold. *J. Gastrointest. Surg. Off. J. Soc. Surg. Aliment. Tract* **13**, 1422–1429 (2009).

4 2. Stoodley, P. *et al.* Tonsillolith. *Otolaryngol. Neck Surg.* **141**, 316–321 (2009).

5 3. Manetti, A. G. O. *et al.* Environmental Acidification Drives S. pyogenes Pilus Expression and

6 Microcolony Formation on Epithelial Cells in a FCT-Dependent Manner. *PLOS ONE* **5**, e13864 (2010).

7 4. Dalton, T. L. & Scott, J. R. CovS Inactivates CovR and Is Required for Growth under Conditions of

8 General Stress in Streptococcus pyogenes. *J. Bacteriol.* **186**, 3928–3937 (2004).

9 5. Chiang-Ni, C., Chiou, H.-J., Tseng, H.-C., Hsu, C.-Y. & Chiu, C.-H. RocA Regulates Phosphatase

10 Activity of Virulence Sensor CovS of Group A Streptococcus in Growth Phase- and pH-Dependent

11 Manners. *mSphere* **5**, e00361-20 (2020).

12 6. Tatsuno, I., Isaka, M., Okada, R., Zhang, Y. & Hasegawa, T. Relevance of the two-component sensor

13 protein CiaH to acid and oxidative stress responses in Streptococcus pyogenes. *BMC Res. Notes* **7**, 189

14 (2014).

15 7. Do, H. *et al.* Environmental pH and peptide signaling control virulence of Streptococcus pyogenes via

16 a quorum-sensing pathway. *Nat. Commun.* **10**, 2586 (2019).

17 8. Chiang-Ni, C., Tseng, H.-C., Hung, C.-H. & Chiu, C.-H. Acidic stress enhances CovR/S-dependent gene

18 repression through activation of the *covR/S* promoter in *emm1*-type group A *Streptococcus*. *Int. J. Med.*

19 *Microbiol.* **307**, 329–339 (2017).

9. Cotter, P. D. & Hill, C. Surviving the acid test: responses of gram-positive bacteria to low pH. *Microbiol. Mol. Biol. Rev. MMBR* **67**, 429–453, table of contents (2003).

10. Ramboarina, S. *et al.* Structural Insights into Serine-rich Fimbriae from Gram-positive Bacteria. *J. Biol. Chem.* **285**, 32446–32457 (2010).

11. Sequeira, S. *et al.* Structural basis for the role of serine-rich repeat proteins from Lactobacillus reuteri in gut microbe–host interactions. *Proc. Natl. Acad. Sci.* **115**, E2706–E2715 (2018).

12. Jacquot, A. *et al.* The dynamics and pH-dependence of Ag43 adhesins' self-association probed by atomic force spectroscopy. *Nanoscale* **6**, 12665–12681 (2014).

13. Taglialegna, A. *et al.* Staphylococcal Bap Proteins Build Amyloid Scaffold Biofilm Matrices in Response to Environmental Signals. *PLOS Pathog.* **12**, e1005711 (2016).

14. Dehinwal, R. *et al.* A pH-sensitive motif in an outer membrane protein activates bacterial membrane vesicle production. *Nat. Commun.* **15**, 6958 (2024).

15. Walden, M. *et al.* An internal thioester in a pathogen surface protein mediates covalent host binding. *eLife* **4**, e06638 (2015).

16. Monzon, V., Lafita, A. & Bateman, A. Discovery of fibrillar adhesins across bacterial species. *BMC Genomics* **22**, 550 (2021).

17. Pointon, J. A. *et al.* A Highly Unusual Thioester Bond in a Pilus Adhesin Is Required for Efficient Host Cell Interaction, *J. Biol. Chem.* **285**, 33858–33866 (2010).

18. Ramachandran, V. *et al.* Two Distinct Genotypes of *prtF2* , Encoding a Fibronectin Binding Protein,

and Evolution of the Gene Family in *Streptococcus pyogenes*. *J. Bacteriol.* **186**, 7601–7609 (2004).

19. Echelman, D. J., Lee, A. Q. & Fernández, J. M. Mechanical forces regulate the reactivity of a thioester bond in a bacterial adhesin. *J. Biol. Chem.* **292**, 8988–8997 (2017).

20. Alonso-Caballero, A. *et al.* Protein folding modulates the chemical reactivity of a Gram-positive adhesin. *Nat. Chem.* **13**, 172–181 (2021).

21. Walden, M., Crow, A., Nelson, M. D. & Banfield, M. J. Intramolecular isopeptide but not internal thioester bonds confer proteolytic and significant thermal stability to the S. pyogenes pilus adhesin Spy0125. *Proteins Struct. Funct. Bioinforma.* **82**, 517–527 (2014).

22. Greenfield, N. J. & Fasman, G. D. Computed circular dichroism spectra for the evaluation of protein conformation. *Biochemistry* **8**, 4108–4116 (1969).

23. Cooper, T. M. & Woody, R. W. The effect of conformation on the CD of interacting helices: A theoretical study of tropomyosin. *Biopolymers* **30**, 657–676 (1990).

24. Rogers, D. M. *et al.* Electronic Circular Dichroism Spectroscopy of Proteins. *Chem* **5**, 2751–2774 (2019).

25. Riener, C. K., Kada, G. & Gruber, H. J. Quick measurement of protein sulfhydryls with Ellman's reagent and with 4,4′-dithiodipyridine. *Anal. Bioanal. Chem.* **373**, 266–276 (2002).

26. Ghassemian, A., Vila-Farrés, X., Alewood, P. F. & Durek, T. Solid phase synthesis of peptide-selenoesters. *Bioorg. Med. Chem.* **21**, 3473–3478 (2013).

27. Abramson, J. *et al.* Accurate structure prediction of biomolecular interactions with AlphaFold 3. *Nature*

630, 493–500 (2024).

28. Matsunaga, R. & Tsumoto, K. FASTIA: A rapid and accessible platform for protein variant interaction analysis demonstrated with a single-domain antibody. *Protein Sci.* **34**, e70065 (2025).

29. Bogan, A. A. & Thorn, K. S. Anatomy of hot spots in protein interfaces1. *J. Mol. Biol.* **280**, 1–9 (1998).

30. Pállinger, E. & Csaba, G. Presence and distribution of biogenic amines (histamine, serotonin and epinephrine) in immunophenotyped human immune cells. *Inflamm. Res. Off. J. Eur. Histamine Res. Soc. Al* **57**, 530–534 (2008).

31. Alberty, R. *Thermodynamics of Biochemical Reactions*. (2003). doi:10.1002/0471332607.

32. Harris, T. K. & Turner, G. J. Structural Basis of Perturbed pKa Values of Catalytic Groups in Enzyme Active Sites. *IUBMB Life* **53**, 85–98 (2002).

33. Whitnack, E. & Beachey, E. H. Antiopsonic activity of fibrinogen bound to M protein on the surface of group A streptococci. *J. Clin. Invest.* **69**, 1042–1045 (1982).

34. Anderson, E. L. *et al.* The Fibrinogen-binding M1 Protein Reduces Pharyngeal Cell Adherence and Colonization Phenotypes of M1T1 Group A Streptococcus*. *J. Biol. Chem.* **289**, 3539–3546 (2014).

35. Kilambi K. P., Reddy K. & Gray J. J. Protein-Protein Docking with Dynamic Residue Protonation States. *PLOS Comput. Biol.* **10**, e1004018 (2014).

36. Keeble, A. H. *et al.* Approaching infinite affinity through engineering of peptide–protein interaction. *Proc. Natl. Acad. Sci.* **116**, 26523–26533 (2019).

37. Zakeri, B. *et al.* Peptide tag forming a rapid covalent bond to a protein, through engineering a bacterial

adhesin. *Proc. Natl. Acad. Sci. U. S. A.* **109**, E690-697 (2012).

38. Predeina, O. *et al.* The SpyBLI cell-free pipeline for the rapid quantification of binding kinetics from crude samples. *RSC Chem. Biol.* **6**, 1313–1327 (2025).

39. Kollman, J. M., Pandi, L., Sawaya, M. R., Riley, M. & Doolittle, R. F. Crystal Structure of Human Fibrinogen. *Biochemistry* **48**, 3877–3886 (2009).

40. Kuhn, B. T. *et al.* Biotinylation of Membrane Proteins for Binder Selections. in *Expression, Purification, and Structural Biology of Membrane Proteins* (eds Perez, C. & Maier, T.) 151–165 (Springer US, New York, NY, 2020). doi:10.1007/978-1-0716-0373-4_11.

41. Virtanen, P. *et al.* SciPy 1.0: fundamental algorithms for scientific computing in Python. *Nat. Methods* **17**, 261–272 (2020).

42. Motulsky, H. & Christopoulos, A. *Fitting Models to Biological Data Using Linear and Nonlinear Regression: A Practical Guide to Curve Fitting*. (Oxford University Press, New York, NY, 2004). doi:10.1093/oso/9780195171792.001.0001.

Extended Data

Extended Data Table 1 | T_m of lower-temperature or higher-temperature peak (mean ± SD, n=3 (WT, C109S, Q261A), n=1 (C109A)).

		T_m 1 (°C)	T_m 2 (°C)
WT	pH 6.0	56.69 ± 0.39	66.54 ± 0.09
	pH 6.5	56.97 ± 0.12	66.44 ± 0.02
	pH 7.0	54.70 ± 0.13	—
	pH 7.3	52.10 ± 0.41	—
	pH 8.0	49.84 ± 0.35	—
C109S	pH 6.0	55.76 ± 0.02	—
	pH 7.3	53.38 ± 0.04	—
Q261A	pH 6.0	55.68 ± 0.23	—
	pH 7.3	53.44 ± 0.09	—
C109A	pH 6.0	52.38	—
	pH 7.3	49.89	—

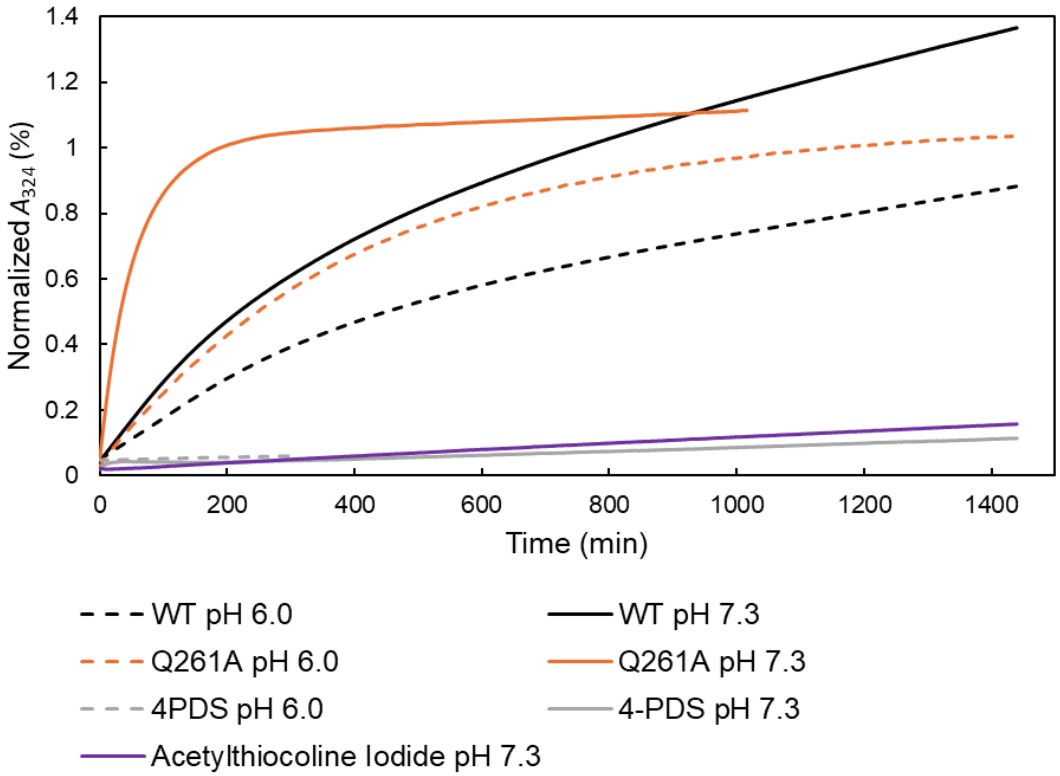

Extended Data Fig. 1 | The reaction of folded SfbI-TED with 4-PDS.

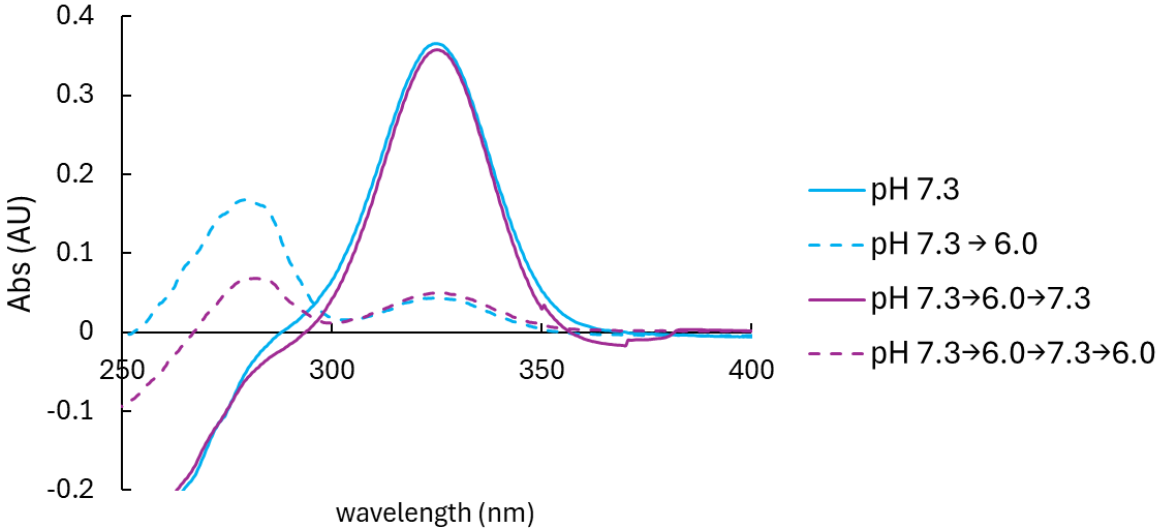

Extended Data Fig. 2 | The retained pH responsiveness after repeated pH cycle.

a.

WT : S E N E D Y Q N L L S A E Y V P

Q261E conversion: S E N E D Y E N L L S A E Y V P

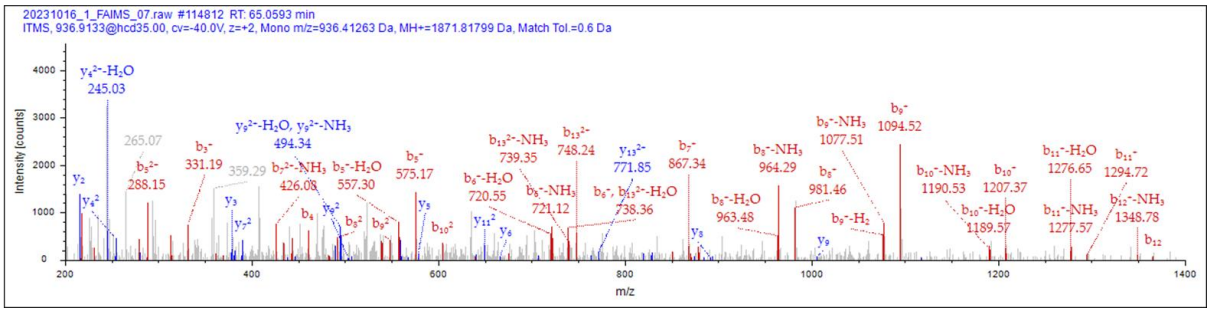

b.

#1	b+	b2+	Seq.	y+	y2+	#2
1	88.03930	44.52329	S			16
2	217.08190	109.04459	E	1784.78612	892.89670	15
3	331.12483	166.06605	N	1655.74352	828.37540	14
4	460.16742	230.58735	E	1541.70060	771.35394	13
5	575.19436	288.10082	D	1412.65800	706.83264	12
6	738.25769	369.63248	Y	1297.63106	649.31917	11
7	867.30028	434.15378	E	1134.56773	567.78750	10
8	981.34321	491.17524	N	1005.52514	503.26621	9
9	1094.42727	547.71728	L	891.48221	446.24474	8
10	1207.51134	604.25931	L	778.39815	389.70271	7
11	1294.54337	647.77532	S	665.31408	333.16068	6
12	1365.58048	683.29388	A	578.28205	289.64467	5
13	1494.62307	747.81517	E	507.24494	254.12611	4
14	1657.68640	829.34684	Y	378.20235	189.60481	3
15	1756.75482	878.88105	V	215.13902	108.07315	2
16			P	116.07061	58.53894	1

Extended Data Fig. 3 | MS/MS analysis of the peptide with a Q261E conversion arising from hydrolysis of the thioester bond.

a, Annotated MS/MS spectrum of the peptide containing a Q261E conversion. **b,** Assignment of b- and y-ion fragment ions supporting the Q261E conversion.

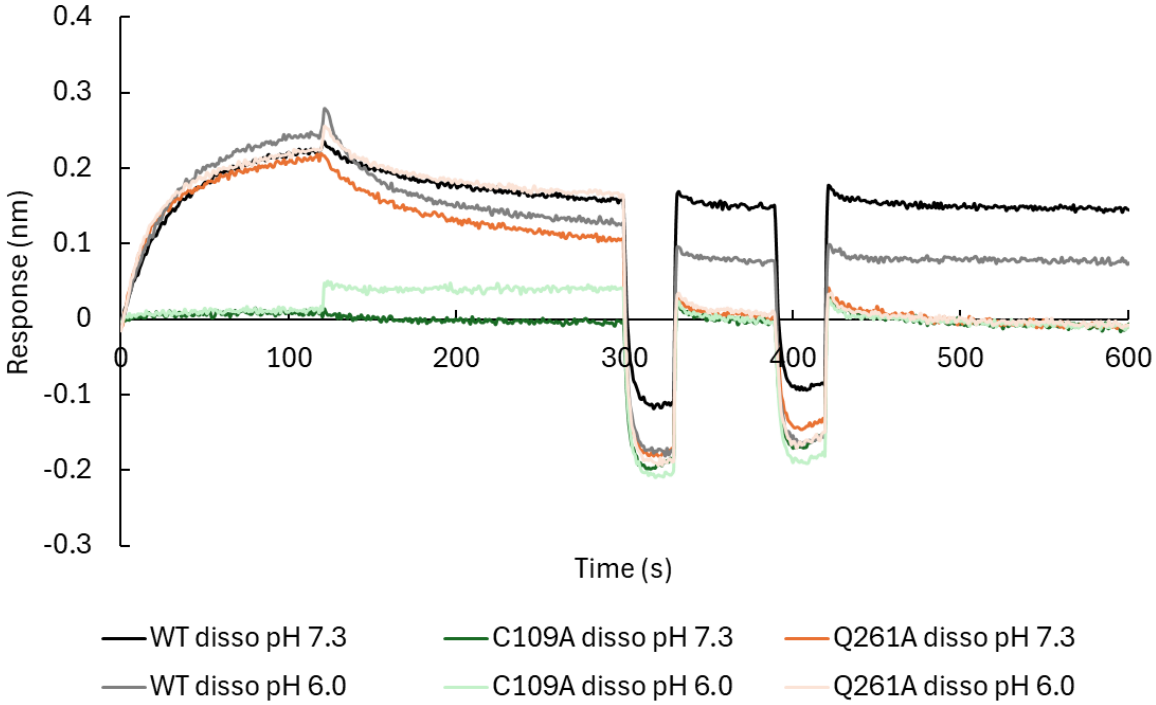

Extended Data Fig. 4 | The raw data of BLI (Fig.3A).

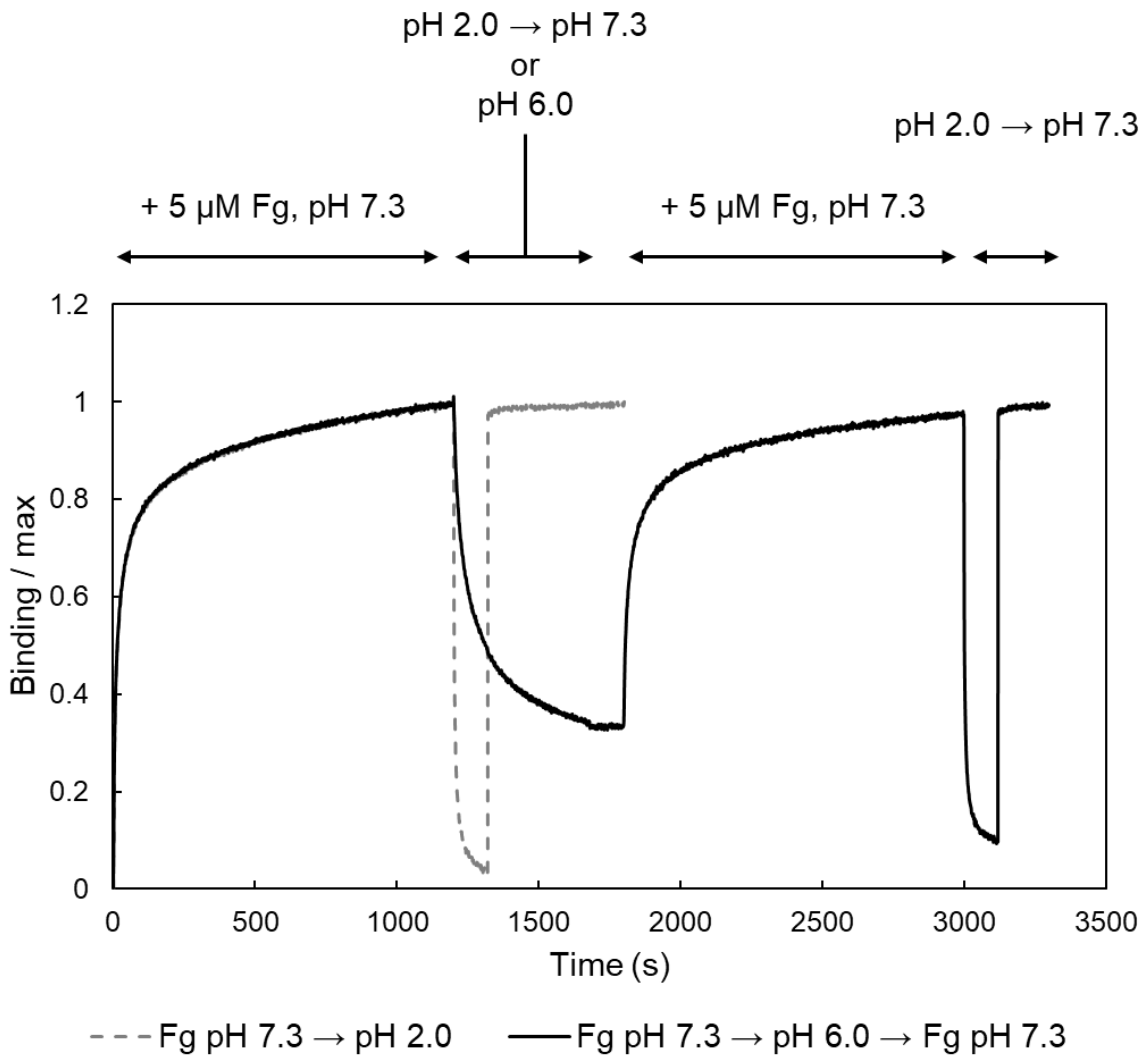

Extended Data Fig. 5 | The amount of intermolecular crosslinked complex formed immediately after the association and dissociation steps.